

PAPER • OPEN ACCESS

## Prediction of Mechanical Behaviors of the Q & P980 Steel Under Different Temperatures and Strain Rates Using Crystal Plasticity Method

To cite this article: Hao Yang *et al* 2020 *IOP Conf. Ser.: Mater. Sci. Eng.* **967** 012016

View the [article online](#) for updates and enhancements.

You may also like

- [The Carnegie Supernova Project. I. Third Photometry Data Release of Low-redshift Type Ia Supernovae and Other White Dwarf Explosions](#)  
Kevin Krisciunas, Carlos Contreras, Christopher R. Burns *et al.*
- [Warm deformation behaviour of P92 steel](#)  
J Obiko, L H Chown and D J Whitefield
- [Influence of Different Weld Heat Input on Microstructure and Properties of New Martensitic Heat-resistant Steel Joints by Automatic Welding](#)  
Yiwei Wang, Wangyu Dong, Jianlu Shang *et al.*



**ECS**  
The  
Electrochemical  
Society  
Advancing solid state &  
electrochemical science & technology

**DISCOVER**  
how sustainability  
intersects with  
electrochemistry & solid  
state science research

# Prediction of Mechanical Behaviors of the Q&P980 Steel Under Different Temperatures and Strain Rates Using Crystal Plasticity Method

Hao Yang<sup>a</sup>, Huamiao Wang<sup>a</sup>, Dayong Li<sup>a,b,\*</sup>, Yinghong Peng<sup>a</sup>, Peidong Wu<sup>c</sup>

<sup>a</sup>State Key Laboratory of Mechanical System and Vibration, Shanghai Jiao Tong University, Shanghai, 200240, China

<sup>b</sup>Materials Genome Initiative Center, Shanghai Jiao Tong University, 200240, China

<sup>c</sup>Department of Mechanical Engineering, McMaster University, Hamilton, Ontario, L8S 4G7, Canada

\*Corresponding author: dyli@sjtu.edu.cn

**Abstract.** The martensitic transformation in quenching and partitioning (Q&P) steels is greatly influenced by loading conditions such as environmental temperature and loading speed, and thus impacts the macroscopic mechanical properties during the deformation process. Within this work, an elastic-visco-plastic self-consistent (EVPSC) framework coupling with phase transformation model is used to simulate the stress strain responses as well as the microstructure evolution of the multi-phases Q&P980 steel under uniaxial tension process. A temperature and strain rate dependent transformation kinetics is incorporated into the model and phase transformation behaviors of the Q&P980 steel under different temperatures (25 °C~100 °C) and strain rates (0.0002s<sup>-1</sup>~2s<sup>-1</sup>) are successfully characterized. The corresponding stress strain responses under different loading conditions are predicted and compared with the experimental data.

## 1. Introduction

As a representative of the 3rd generation advanced high strength steels (3G-AHSS), Q&P steels possess good combination of strength and ductility and offers great potential in forming light-weight vehicle structures [1]. The Q&P concept was originally proposed by Speer et al. [2] and has been explored for years [3]. The Q&P980 steel has been commercialized for fabrication of automotive structural and safety parts such as cross members, longitudinal beams, B-pillar reinforcements, sills, and bumper reinforcements [4].



There are three phases in Q&P980 steel at the initial state: retained austenite (RA), ferrite (F) and tempered martensite (TM). During deformation, phase transformation occurs from RA to newly formed martensite (NM), enhancing the ductility and strength. Under press forming process of sheet metal, the strain rate is in the range of 0.1~10 s<sup>-1</sup> and the temperature rising due to plastic work is below 100 °C. These variant environmental conditions affect the transformation behaviors and impact the mechanical behaviors.

An EVPSC framework coupling with phase transformation model is used to study phase transformation behaviors of the Q&P980 steel under different temperatures and strain rates, and predict the macroscopic flow stress behaviors. The microstructure evolution is also characterized by the model and compared with experimental results.

## 2. Experiment

Experimental results from Hu et al. [5] and Zou et al. [6] were used in this study. The lattice strain evolution of each phase during tension is from Hu et al. [5]. Phase transformation behaviors and stress strain responses under different temperatures and strain rates are from Zou et al. [6]. Both of the Q&P980 steels in the literature are from BAOSTEEL. The chemical composition, microstructure characterization and quasi-static uniaxial tension stress strain curves of the two steels were compared and little difference was found. Therefore, the experimental data could be used together.

## 3. Model description

A crystallographic phase transformation model was implemented into an EVPSC [7, 8] framework, which can be summarized as follows:

For each crystal, the total strain rate is divided by elastic strain ( $\dot{\boldsymbol{\epsilon}}^e$ ) and plastic strain. The plastic strain consists of crystal slip ( $\dot{\boldsymbol{\epsilon}}^p$ ) and transformation strain ( $\dot{\boldsymbol{\epsilon}}^{pt}$ ).

$$\dot{\boldsymbol{\epsilon}}^p = \dot{\gamma}_0 \sum_{\alpha} \mathbf{P}^{\alpha} \left| \frac{\tau^{\alpha}}{\tau_{cr}^{\alpha}} \right|^{\frac{1}{m}-1} \frac{\tau^{\alpha}}{\tau_{cr}^{\alpha}} \quad (1)$$

where  $\dot{\gamma}_0$  is the reference value for the slip rate;  $m$  the rate sensitivity,  $\mathbf{P}^{\alpha}$  the Schmid tensor.  $\tau^{\alpha}$

and  $\tau_{cr}^{\alpha}$  are the resolved shear stress (RSS), and the critical resolved shear stress (CRSS), respectively.

$\tau_{cr}^{\alpha}$  is characterized in the form of modified Voce hardening law [9]:

$$\tau_{cr}^{\alpha} = \tau_0^{\alpha} + (\tau_l^{\alpha} + \theta_l^{\alpha} \Gamma) (1 - \exp(-\Gamma \left| \frac{\theta_0^{\alpha}}{\tau_l^{\alpha}} \right|)) \quad (2)$$

where  $\Gamma = \sum_{\alpha} \dot{\gamma}^{\alpha}$  is the accumulated shear in the grain,  $\tau_0^{\alpha}$  the initial CRSS,  $\theta_0^{\alpha}$  the initial hardening

rate,  $\theta_l^{\alpha}$  the asymptotic hardening rate, and  $(\tau_0^{\alpha} + \tau_l^{\alpha})$  the back-extrapolated CRSS, respectively.

For the ferrite and martensite grains, there is no transformation strain ( $\dot{\boldsymbol{\epsilon}}^{pt}=0$ ). For the austenite grains, strain-induced martensitic transformation (SIMT) can occur and induce transformation strain

when the accumulated shear exceeds a critical value.

The phase transformation model can be summarized as follows:

- (1) For an austenite grain that has not experienced phase transformation, if the accumulated shear of the grain reaches a critical value  $\Gamma_c$ , then the transformation of the grain will initiate.
- (2) There are 24 possibly formed martensite variants, according to the K-S orientation relationship, but only the one with the maximum transformation energy potential ( $U_i = \sigma : \boldsymbol{\varepsilon}_i^{PT}, i = 1, \dots, 24$ ) is chosen as the nucleation of NM.
- (3) If a transformation martensite grain is nucleated, its initial stress state is set to be equal to the current parent austenite grain considering the stress balance, and its initial shape is set to be a plate-like with axis ratio of 10:10:1, based on the experimental observation [10].
- (4) If one variant is selected, other variants will be restricted. This assumption is not only based on experimental results [11] but also on common sense that growing up on an existing nucleus is much easier than nucleation again.
- (5) A modified phenomenological transformation kinetics equation is used to describe the volumetric evolution of an austenite grain.

$$f = 1 - \exp\{-\beta[1 - \exp(\alpha\Gamma)]^2\} \quad (3)$$

where  $\alpha(T, \dot{\boldsymbol{\varepsilon}})$  and  $\beta(T, \dot{\boldsymbol{\varepsilon}})$  are transformation parameters.

- (6) The transformation associated dilatational and shear strains are about 3.7% and 22%, respectively.

The Eigen transformation strain tensor  $\boldsymbol{\varepsilon}^{PT}$  of the variant with  $(011)_{\alpha} // (111)_{\gamma}$  and  $[11\bar{1}]_{\alpha} // [10\bar{1}]_{\gamma}$  is given by (referred to austenitic axes)

$$\boldsymbol{\varepsilon}^{PT} = \frac{(F^T F - I)}{2} = \begin{bmatrix} -0.0061 & 0 & -0.0242 \\ 0 & 0.131 & 0 \\ -0.0242 & 0 & -0.0958 \end{bmatrix} \quad (4)$$

The transformation strain tensors of other variants are calculated by multiplication of  $\boldsymbol{\varepsilon}^{PT}$  with associated crystal symmetry operation matrices.

A uniform macroscopic strain is imposed on a material point. An aggregate of 10000 grains is considered for the Q&P980 alloy, and consists of four phases: RA, F, TM and NM. According to Zou et al. [6], the volume fractions of the RA, F, TM and NM are taken to be respectively 10.6% (1060 grains), 37.5% (3750 grains), 51.9% (5190 grains) and zero at the initial state. The initial texture measured by electron backscatter diffraction (EBSD) is used as input for each phase. For the RA, 12  $\{111\}\langle 110 \rangle$  slip systems are used without considering the twinning mechanism. For the F, TM and NM, the 12  $\{110\}\langle 111 \rangle$  and 12  $\{112\}\langle 111 \rangle$  slip systems are used in this study. The single-crystal elastic constants for the  $\gamma$  (RA) and  $\alpha$  (F, TM and NM) phases are set to be:  $C_{11}^{\gamma} = 209\text{GPa}$ ,  $C_{12}^{\gamma} = 133\text{GPa}$ ,

$C_{44}^{\gamma} = 121\text{GPa}$  [12] and  $C_{11}^{\alpha} = 222\text{GPa}$ ,  $C_{12}^{\alpha} = 143\text{GPa}$ ,  $C_{44}^{\alpha} = 114\text{GPa}$  [13], respectively. The calibrated model parameters of each phase are listed in Table 1.

**Table 1** Model parameters

phase	Slip mode	$\tau_0$	$\tau_1$	$\theta_0$	$\theta_1$
RA	{111}<110>	380	1	800	20
F	{110}<111>	190	150	1200	150
	{112}<111>	190	150	1200	150
TM	{110}<111>	380	50	600	50
	{112}<111>	380	50	600	50
NM	{110}<111>	450	40	2500	2200
	{112}<111>	450	40	2500	2200

#### 4. Results

The stress strain responses as well as the volumetric evolution of RA is shown in Figure 1a. The volume fraction of RA continues decreasing to 6% at  $\epsilon=0.15$ . The lattice strain of each phase during deformation is shown in Figure 1b. After yielding, the F and NM show obvious hardening behavior, while the lattice strains of RA and TM almost do not change. The texture of each phase after 15% tension is shown in Figure 2. After deformation, the <111> fiber texture of RA and the <110> fiber texture of F and TM enhanced. The current model is able to reproduce the macroscopic mechanical properties as well as microstructure evolutions of the multi-phase Q&P980 steel.

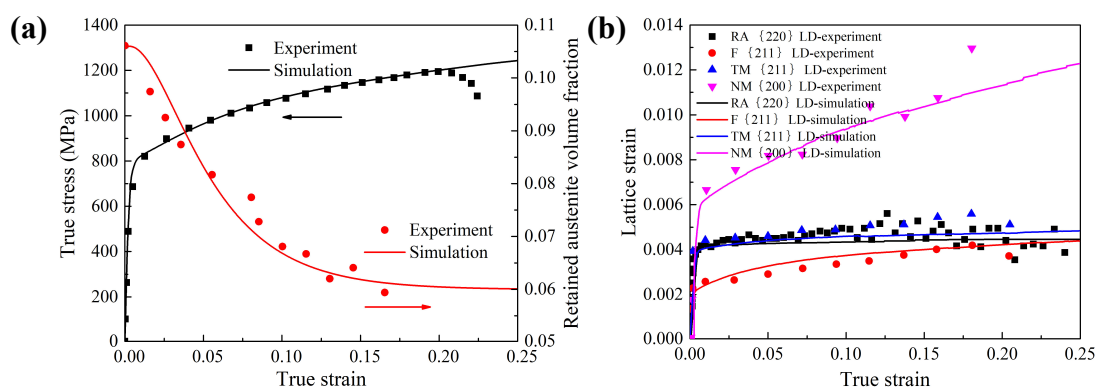


**Figure 1.** (a) experimental and simulated flow stress and volumetric evolution of RA, (b) experimental and simulated lattice strain evolution of each phase

	Experiment	Simulation
--	------------	------------

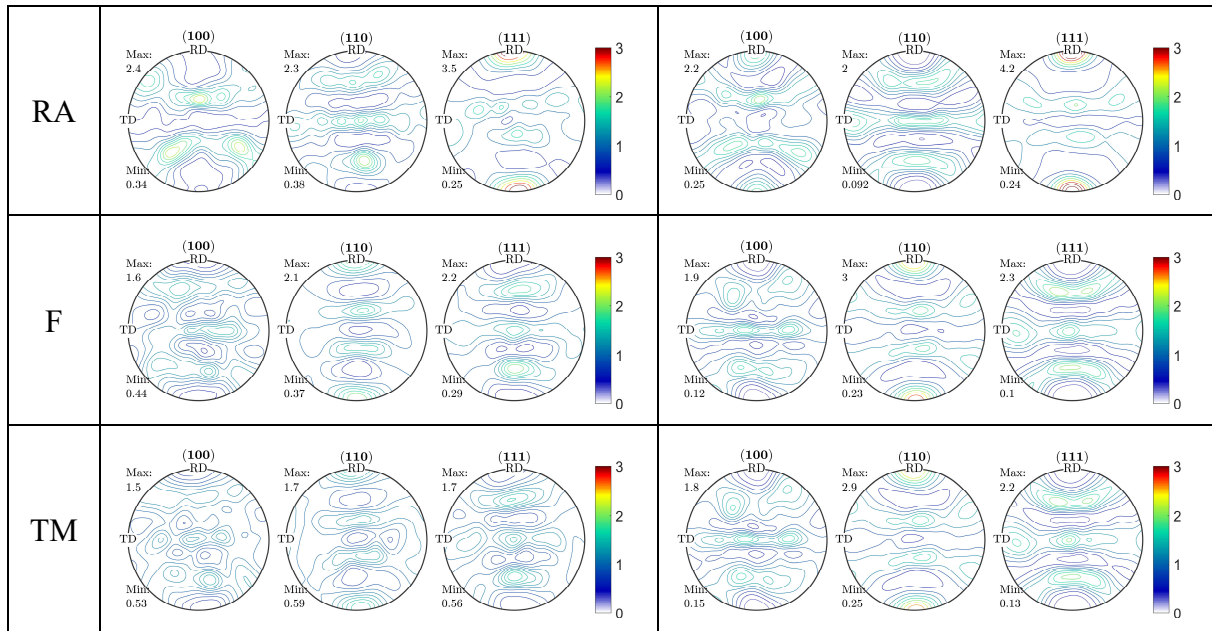


**Figure 2.** experimental and simulated texture at 15% strain

The relationship between transformation parameters ( $\alpha$ ,  $\beta$ ) and loading conditions ( $T$ ,  $\dot{\epsilon}$ ) is given by:

$$\alpha = 2.2f_1f_2 - 12.7956(f_1 + f_2) + 80.0012 \quad (5)$$

where  $f_1 = -0.005T + 6.36$ ,

$$f_2 = -0.0003(\ln \dot{\epsilon})^4 + 0.0035(\ln \dot{\epsilon})^3 + 0.17(\ln \dot{\epsilon})^2 + 1.31 \ln \dot{\epsilon} + 8.8$$

$$\beta = 0.81g_1g_2 - 0.8132(g_1 + g_2) + 0.4585 \quad (6)$$

where  $g_1 = -0.0047T + 0.65$ ,

$$g_2 = 0.000546(\ln \dot{\epsilon})^4 + 0.0107(\ln \dot{\epsilon})^3 + 0.0757(\ln \dot{\epsilon})^2 + 0.1988 \ln \dot{\epsilon} + 0.52222$$

The phase transformation behaviors and stress strain responses under different temperatures (where  $\dot{\epsilon} = 0.0002 \text{ s}^{-1}$ ) are shown in [Figure 3a](#) and [Figure 3b](#), respectively. With temperature increasing, phase transformation is constrained and the strength is weakened. The phase transformation behaviors and stress strain responses under different strain rates (where  $T = 25^\circ\text{C}$ ) are shown in [Figure 4a](#) and [Figure 4b](#), respectively. With strain rate increasing, phase transformation is constrained firstly but enhanced after  $\dot{\epsilon} > 0.1 \text{ s}^{-1}$ . Therefore, the strength is not enhanced with strain rate monotonously and the flow stress crosses with each other at low strain rate ( $\dot{\epsilon} < 0.1 \text{ s}^{-1}$ ).

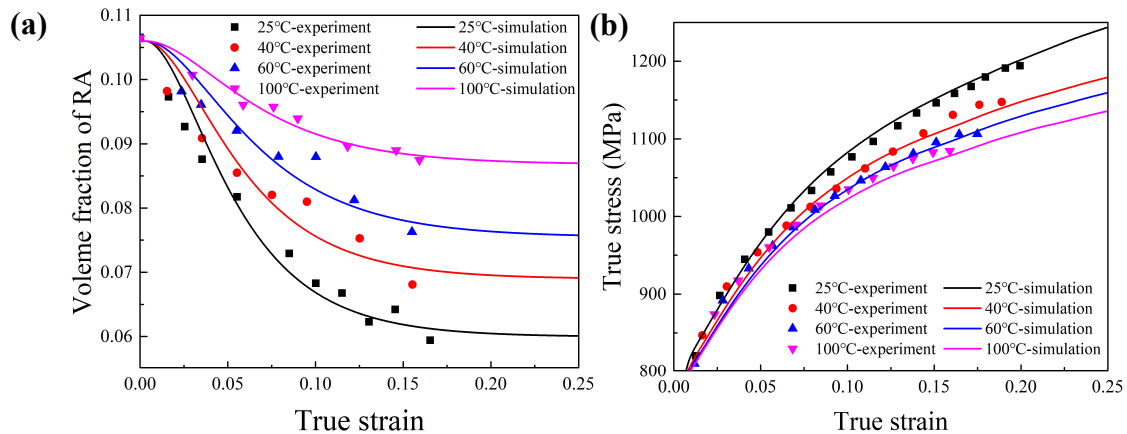


**Figure 3.** (a) measured and simulated volume fraction of RA under different temperatures, (b) measured and simulated stress strain responses under different temperatures

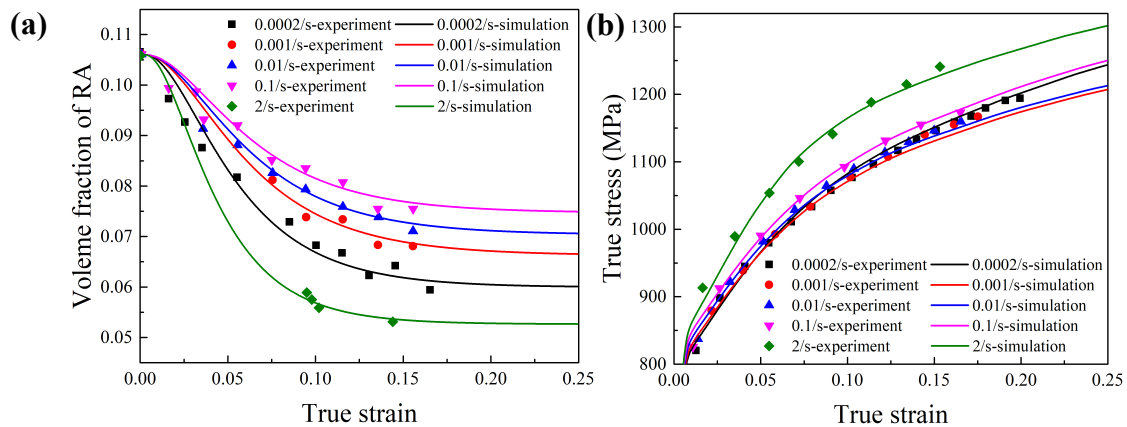


**Figure 4.** (a) measured and simulated volume fraction of RA under different strain rates, (b) measured and simulated stress strain responses under different strain rates

## 5. Conclusions

An EVPSC framework was combined with crystallographic phase transformation model to capture the macroscopic mechanical behavior as well as microstructure evolutions of the Q&P980 steel. The developed model was able to characterize the phase transformation behaviors and predict the stress strain responses under different temperatures and strain rates.

## Acknowledgements

DL acknowledges the support by NSFC [Grant number U1860110]. The original EBSD data was supplied by D. Q. Zou et al.

## References

- [1] D.K. Matlock, Speer, J.G., Third generation of AHSS: microstructure design concepts, microstructure and texture in steels, 2009.
- [2] J. Speer, D.K. Matlock, B.C. De Cooman, J.G. Schroth, Carbon partitioning into austenite after martensite transformation, *Acta Materialia* 51(9) (2003) 2611-2622.

- [3] L. Wang, W. Feng, Development and Application of Q&P Sheet Steels, 2011.
- [4] L. Wang, J.G. Speer, Quenching and Partitioning Steel Heat Treatment, Metallography, Microstructure, and Analysis 2(4) (2013) 268-281.
- [5] X.H. Hu, X. Sun, L.G. Hector, Y. Ren, Individual phase constitutive properties of a TRIP-assisted QP980 steel from a combined synchrotron X-ray diffraction and crystal plasticity approach, Acta Materialia 232 (2017) 230-244.
- [6] D.Q. Zou, S.H. Li, J. He, Temperature and strain rate dependent deformation induced martensitic transformation and flow behavior of quenching and partitioning steels, Materials Science and Engineering: A 680 (2017) 54-63.
- [7] H. Wang, P.D. Wu, C.N. Tomé, Y. Huang, A finite strain elastic–viscoplastic self-consistent model for polycrystalline materials, Journal of the Mechanics and Physics of Solids 58(4) (2010) 594-612.
- [8] H. Wang, Y. Jeong, B. Clausen, Y. Liu, R.J. McCabe, F. Barlat, C.N. Tomé, Effect of martensitic phase transformation on the behavior of 304 austenitic stainless steel under tension, Materials Science and Engineering: A 649 (2016) 174-183.
- [9] C. Tome, G.R. Canova, U.F. Kocks, N. Christodoulou, J.J. Jonas, The relation between macroscopic and microscopic strain hardening in F.C.C. polycrystals, Acta Metallurgica 32(10) (1984) 1637-1653.
- [10] S. Turteltaub, A.S.J. Suiker, Transformation-induced plasticity in ferrous alloys, Journal of the Mechanics and Physics of Solids 53(8) (2005) 1747-1788.
- [11] N. Gey, B. Petit, M. Humbert, Electron backscattered diffraction study of  $\epsilon/\alpha'$  martensitic variants induced by plastic deformation in 304 stainless steel, Metallurgical & Materials Transactions A 36(12) (2005) 3291-3299.
- [12] H.M. Ledbetter, Predicted monocrystal elastic constants of 304-type stainless steel, Physica B & C 128B+C(1) (1985) 1-4.
- [13] M.R. Fellingner, L.G. Hector, D.R. Trinkle, Effect of solutes on the lattice parameters and elastic stiffness coefficients of body-centered tetragonal Fe, Computational Materials Science 152 (2018) 308-323.